Article

Ru/Ce/Ni Metal Foams as Structured Catalysts for the Methanation of CO$_2$

Stefano Cimino [1,*], **Elisabetta Maria Cepollaro** [1], **Luciana Lisi** [1], **Stefano Fasolin** [2], **Marco Musiani** [2] **and Lourdes Vázquez-Gómez** [2]

[1] Istituto di Scienze e Tecnologie per l'Energia e la Mobilità Sostenibili (STEMS),
    Consiglio Nazionale delle Ricerche (CNR), Via Guglielmo Marconi 4/10, 80125 Napoli, Italy;
    elisabettamaria.cepollaro@unina.it (E.M.C.); luciana.lisi@stems.cnr.it (L.L.)
[2] Istituto di Chimica della Materia Condensata e di Tecnologie per l'Energia (ICMATE),
    Consiglio Nazionale delle Ricerche (CNR), Corso Stati Uniti 4, 35127 Padova, Italy;
    stefano.fasolin@cnr.it (S.F.); marco.musiani@cnr.it (M.M.); lourdes.vazquezgomez@cnr.it (L.V.-G.)
*   Correspondence: stefano.cimino@cnr.it

Abstract: The development of highly conductive structured catalysts with enhanced mass- and heat-transfer features is required for the intensification of the strongly exothermic catalytic hydrogenation of CO$_2$ in which large temperature gradients should be avoided to prevent catalyst deactivation and to control selectivity. Therefore, in this work we set out to investigate the preparation of novel structured catalysts obtained from a commercial open cell Ni foam with high pore density (75 ppi) onto which a CeO$_2$ layer was deposited via electroprecipitation, and, eventually, Ru was added by impregnation. Composite Ru/Ce/Ni foam catalysts, as well as simpler binary Ru/Ni and Ce/Ni catalysts were characterized by SEM-EDX, XRD, cyclic voltammetry, N$_2$ physisorption, H$_2$-temperature programmed reduction (TPR), and their CO$_2$ methanation activity was assessed at atmospheric pressure in a fixed bed flow reactor via temperature programmed tests in the range from 200 to 450 °C. Thin porous CeO$_2$ layers, uniformly deposited on the struts of the Ni foams, produced active catalytic sites for the hydrogenation of CO$_2$ at the interface between the metal and the oxide. The methanation activity was further boosted by the dispersion of Ru within the pores of the CeO$_2$ layer, whereas the direct deposition of Ru on Ni, by either impregnation or pulsed electrodeposition methods, was much less effective.

Keywords: CO$_2$ utilization; hydrogenation; methane; electrodeposition; electroprecipitation; ruthenium; ceria; nickel; open cell foams; supported catalysts

1. Introduction

Power-to-Gas (PtG) is a valuable technological option in order to foster the transition to renewable energy sources, representing a strategy for CO$_2$ capture and utilization as well as a chemical storage of energy [1]. To this aim, the hydrogen produced by renewable energy surplus via water electrolysis can be reacted with CO$_2$ (captured from power plants, industrial or biogenic processes) and catalytically transformed to methane (or Substitute Natural Gas, SNG) [1,2] via the well-known Sabatier reaction (Equation (1))

$$CO_2 + 4H_2 \leftrightarrow CH_4 + 2H_2O \qquad \Delta H = -165 \text{ kJ mol}^{-1} \qquad (1)$$

The process has recently attracted a renewed research interest for catalyst innovation with most efforts focused on improving the low-temperature activity of the catalysts (traditionally based on supported Ni and Ru) as well as their long-term stability and anti-sintering properties [2–9]. However, due to the high exothermicity and the equilibrium nature of the Sabatier reaction, a serious challenge in catalytic reactor design is to remove the heat produced and keep a relatively low process temperature without generating

hot spots [5–7]. Therefore, the commercial process for SNG production makes use of adiabatic, packed bed reactors in series with inter-stage cooling and/or large product gas recycling [4,5].

Due to their outstanding heat- and mass-transfer features, coupled to high thermal and mechanical stability as well as low pressure drops, metallic foams are a valuable choice to contrast hot spot formation and reduce the size of the reactor needed to reach high conversions [10,11] when dealing with highly exothermic and possibly diffusion limited processes such as catalytic combustion [12–14], catalytic partial oxidation [15–20], and methanation [7,21–24]. More generally, highly conductive structured catalysts are promising for the intensification of a number of existing strongly exothermic/endothermic catalytic processes in which large temperature gradients should be avoided to prevent catalyst deactivation and to control selectivity [25].

In particular, it has been shown by both computational fluid dynamics calculations and experimental measurements that a large reduction in the "hotspot" temperature along the catalytic bed during methanation can be achieved by using structured catalysts based on reticulated Al- and Ni- open foam substrates, owing to their high thermal conductivity [7,21,23,24].

The preparation of a structured catalyst starting from an open foam metallic substrate is not a trivial matter [10,25] and generally requires the deposition of a thin, uniform, firmly anchored washcoat layer of refractory oxides (such as Al_2O_3, CeO_2, ZrO_2) [20,25] where nanosized active components are then dispersed. Traditional dip-coating procedures may be cumbersome and lead to pore blocking, inhomogeneous distribution, and poor adhesion [10,25]. Hence, alternative methods for efficiently embedding catalytic active components onto the foam substrates are particularly desirable [15]. In particular, taking advantage of the metallic nature of foams, some simple preparation methods such as electrochemically induced precipitation [13,14,16,17] or electrodeposition [12,13,20] have been shown capable to form well-dispersed active layers strongly interacting with the substrate.

In this work we set out to investigate the preparation and CO_2 methanation activity of novel structured catalysts obtained from a commercial open cell Ni foam with high pore density (75 ppi) onto which a CeO_2 layer was deposited via electroprecipitation, and, eventually Ru was added by impregnation. CeO_2 was selected for the ability to vary its oxygen concentration without changing phase, providing a large concentration of active sites for the adsorption and activation of oxygen-containing molecules such as CO_2. In particular, CeO_2 was reported to be among the most effective supports (including γ-Al_2O_3, SiO_2, TiO_2, and ZrO_2) in order to maximize the CO_2 methanation activity of both Ni- and Ru-based catalysts [5,6,26–28].

Electroprecipitation is a versatile method that allows deposition of CeO_2 on various conductive substrates. As the formation of solid deposits is caused by a local pH increase triggered by reduction reactions that produce hydroxide ions, electroprecipitation may be realized on both inert [29–34] and corrodible substrates [35–40]. We have shown that complex-shape 3D substrates, like foams, may be effectively coated [13]. A complex mechanism leading from Ce(III) ions to solid CeO_2, possibly containing minor amounts of Ce(OH)$_3$, has been proposed [13,30,31,33]. The layer thickness may be controlled via the transferred charge [39], although a simple linear relationship between thickness and charge cannot be assumed. While very thin CeO_2 layers are continuous [13,32], cracked deposits form when their thickness is in the micrometers range [35,37,38,40]. This limits the interest of CeO_2 layers for corrosion protection, but is not expected to negatively affect catalysis, especially when the CeO_2-coated foam material is active towards the chosen reaction.

Accordingly, we pursued strong interactions among the composite structured catalyst components, i.e., between Ni foam and CeO_2, between Ru and CeO_2, and between the two metals, Ni and Ru, in order to develop additional active sites for CO_2 methanation.

2. Results and Discussion

2.1. Characterization of the Catalysts

To obtain $Ru/CeO_2/Ni$ catalysts, Ru was deposited onto precut Ni foam disks modified by CeO_2 layers prepared by electroprecipitation [18–30], as schematically depicted in Figure 1.
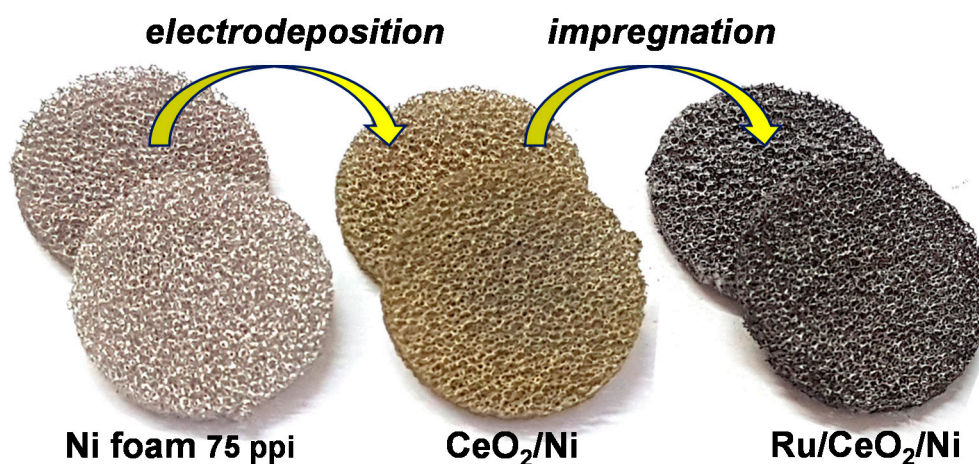
Figure 1. Images of the structured catalysts prepared starting from commercial Ni open cell foam disks with 75 pores per inch (ppi), via CeO_2 electroprecipitation and impregnation with Ru.
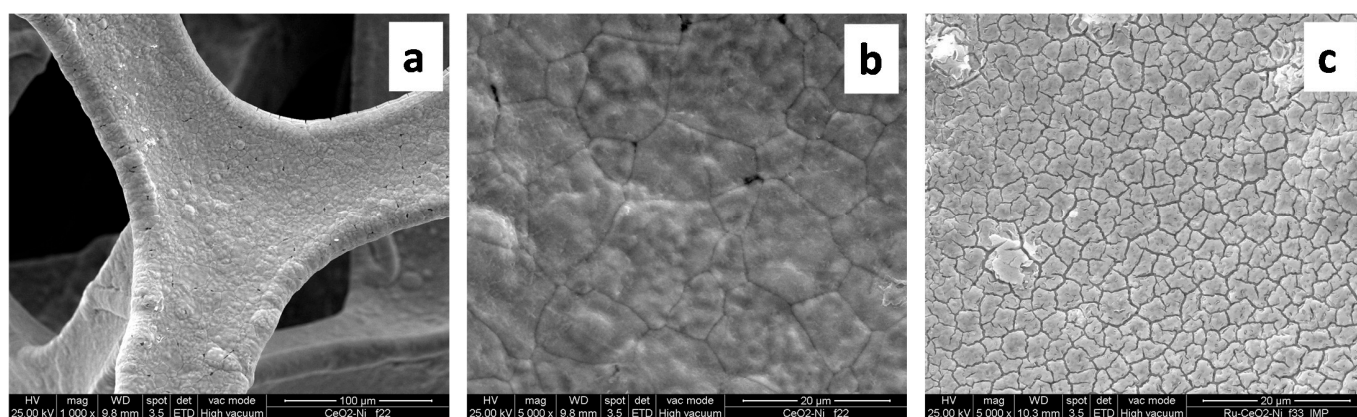
Table 1 presents a summary of the prepared catalysts. Catalysts containing ceria are labeled $Ru/Ce_x/Ni$, where the subscript x refers to the charge (in $C\ cm^{-3}$) used for the deposition of CeO_2.

Table 1. Composition, specific surface area (S.S.A.), and H_2 consumption during temperature programmed reduction (TPR) experiments of the investigated foam catalysts.

Catalyst	CeO_2 Loading mg cm^{-3}	Ru Deposition Method	Ru Loading mg cm^{-3}	S.S.A. [a] m^2 g$_{catalyst}$$^{-1}$	S.S.A. [a,b] m^2 g$_{CeO_2}$$^{-1}$	H_2 Consumption [d] mmol g$_{catalyst}$$^{-1}$
Ni	—	—	—	0.085 [c]		0.05 ± 0.005
Ru/Ni-PED	—	Pulsed Electrodeposition	2.5 (EDS)			0.14 ± 0.01
Ru/Ni	—	Impregnation	7.3			0.22 ± 0.02
Ce$_{12}$/Ni	6.7 ± 1.8	—	—	1.6 ± 0.1	47 ± 12	0.14 ± 0.04
Ce$_{36}$/Ni	23 ± 2	—	—	7.3 ± 0.3	67 ± 10	0.27 ± 0.04
Ru/Ce$_{12}$/Ni	6.7 ± 1.8	Impregnation	7.3	1.8 ± 0.1	57 ± 15	0.26 ± 0.07
Ru/Ce$_{36}$/Ni	23 ± 2	Impregnation	7.3	3.8 ± 0.2	39 ± 6	0.39 ± 0.06

[a] Measured by N_2 adsorption on foam samples after catalytic testing and referred to the total catalyst mass, including Ni foam, CeO_2 and Ru when present. [b] Based on the nominal CeO_2 content of the "as-prepared" foams before the eventual deposition of Ru. [c] Determined by cyclic voltammetry. [d] During H_2-TPR experiments on foam samples preoxidized in air at 300 °C for 1 h.

SEM images of as-prepared Ce_{12}/Ni and $Ru/Ce_{12}/Ni$ are collected in Figure 2. The lower-magnification image (Figure 2a) shows that the CeO_2 layer covers homogeneously the struts of the Ni foam, independently of their position in the inner/outer parts of the disc. At higher magnification (Figure 2b), a few defects are detected, together with the traces of the boundaries between the crystals that constitute the foam, still visible due to the moderate thickness of ceria (0.3–1 μm). Loading with Ru does not induce major changes in the morphology of Ce_{12}/Ni (Figure 2c) except a marked cracking, probably caused by the stresses induced by thermal treatments (at 120 °C and eventually at 450 °C) due to the mismatch between the thermal expansion coefficients of the metal and oxide phases.

Figure 2. SEM images of as-prepared Ce_{12}/Ni (**a**,**b**) and $Ru/Ce_{12}/Ni$ (**c**).

In agreement with previous reports [35,37,38,40], the thicker CeO_2 layers (1.5–3.5 μm) formed on Ce_{36}/Ni samples are porous and heavily cracked, as shown by Figure S1a in the Supplementary Information. Upon Ru loading, $Ru/Ce_{36}/Ni$ samples exhibit areas where significant detachment of the oxide from Ni has occurred (Figure S1b). Part of the detached CeO_2 scales are trapped inside the cells of the foam (Figure S1c).
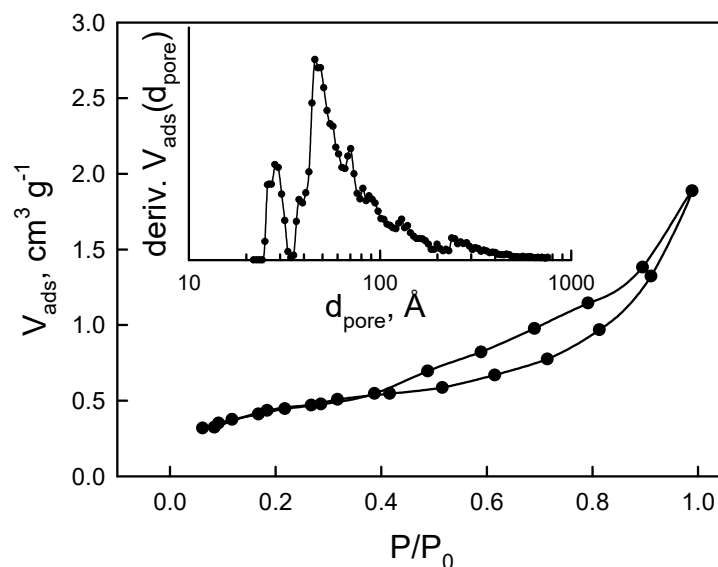
SEM images of CeO_2-free foam catalysts are shown in the Supplementary Information (Figure S2). Discontinuous layers of Ru with a low surface area were present in Ru/Ni. They probably formed via a Ru-Ni galvanic displacement reaction [18] and were possibly modified by the H_2 reduction and thermal treatment. More continuous Ru layers were produced by a pulsed electrodeposition (PED) procedure which also caused Ni dissolution at the grain boundaries at the positive potential limit. In some areas, irregularly distributed on the foam, Ru deposits, hundreds of nanometers wide, were formed onto significantly roughened Ni (Figure S2d). The Ru surface areas measured for Ru/Ni and Ru/Ni-PED samples were respectively 0.011 ± 0.001 and 0.056 ± 0.005 m^2 g^{-1} (referred to the whole catalyst mass). Cyclic voltammograms are shown in Figure S3. These figures confirm the larger Ru coverage of the Ni foam obtained by PED. However, in both cases the Ru surface area remained below that of Ni, a disappointing result at variance with those observed in the galvanic displacement of Ni by other metals, e.g., Pd [41], Rh and Pt [18], which formed well-dispersed, large-area nanometric deposits.

XRD spectra of Ce_x/Ni and $Ru/Ce_x/Ni$ foam catalysts after the reductive pretreatment (Figure S4a) show the presence of sharp peaks at 44.5, 51.8, and 76.3° corresponding to metallic Ni (card 4-850) accompanied by rather small signals at ca. 28.6, 47.6, and 56.4° that can be assigned to the presence of CeO_2 (card 43-1002). No peaks related to Ru can be identified, suggesting that Ru is present in a highly dispersed or amorphous form, although the close proximity of the Ni and Ru main peaks and the much lower content of the latter may be alternative reasons for the lack of clear Ru signals. In fact, also the XRD spectra relevant to Ru/Ni and Ru/Ni-PED samples show no clear signals due to crystalline Ru (Figure S4b), in spite of their rather large deposits detected by SEM analysis, further confirming amorphous nature.

The N_2 adsorption isotherms for Ce_x/Ni and $Ru/Ce_x/Ni$ foams (shown in Figure 3) can be classified as Type IVb, which is typical of mesoporous materials showing some capillary condensation accompanied by a hysteresis on the desorption branch. Considering the negligible contribution from the exposed geometric surface area of the bare Ni structure (0.085 m^2 g^{-1} Table 1), the overall specific surface area can be completely ascribed to the presence of CeO_2: accordingly, it generally increased along with the ceria loading up 7.3 m^2 g^{-1} for those samples with the thicker oxide coat (Table 1). In particular, considering the uncertainty related to the (low) actual oxide loading on the foams, the CeO_2 layer was characterized by a S.S.A. comprised in the range 45–70 m^2 g^{-1}. This figure is roughly independent of the CeO_2 loading and agrees well with recent data on a Pd/CeO_2 catalyst electrodeposited on Fecralloy foams [14]. The pore size distribution
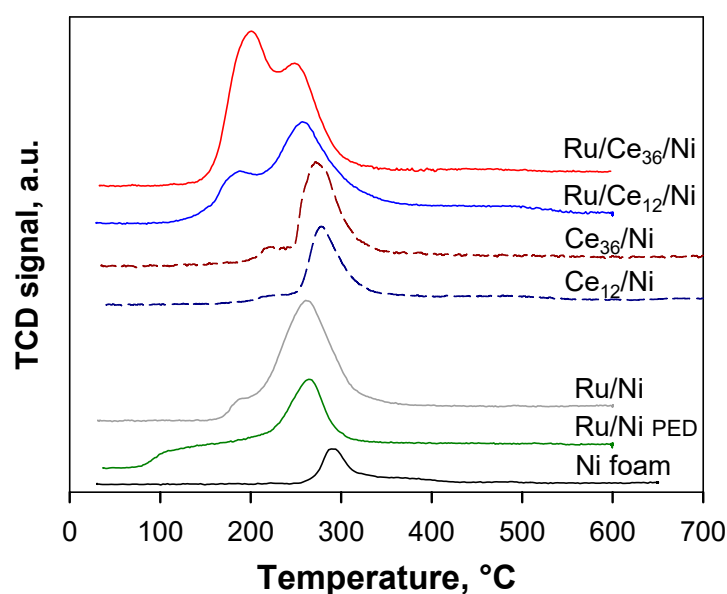
(inset in Figure 3) extended from 25 to 250 Å with the main peak at ca. 50 Å and a further contribution centered at ca. 30 Å, giving a total pore volume of ca. 0.11 ± 0.02 cm^3 g^{-1}. The deposition of Ru onto Ce$_{12}$/Ni foams did not modify significantly the specific surface area of the catalysts (Table 1). The apparent reduction of the specific surface area recorded for Ru/Ce$_{36}$/Ni samples compared to their Ce$_{36}$/Ni counterparts was probably due to some (uncontrolled) loss of the oxide by detachment from the Ni foam occurring either during the Ru-deposition step or (more likely) during the recovery after the catalytic testing. This agrees with SEM analysis of those Ru/Ce$_{36}$/Ni (Figure S1c) showing some detached CeO$_2$ platelets trapped in the cavities of the foams.

Figure 3. N$_2$ adsorption isotherm at 77K over Ce$_{12}$/Ni foam catalyst (the adsorbed volume is referred to total weight). The insert shows the corresponding pore size distribution analysis by the NLDFT method applied to the desorption branch of the isotherm.

H$_2$-temperature programmed reduction (TPR) experiments (Figure 4) were performed to clarify the interactions between phases and the reducibility of the catalysts that is known to play an important role for the CO$_2$ methanation catalytic activity [9]. As a result, the bare Ni foam showed a weak signal in the temperature range from ca. 210 °C up to 350 °C (peak at ca. 290 °C), which did not change significantly in intensity upon the pre-treatment of the foam in air at 300 °C. This peak can be ascribed to the reduction of a small amount of NiO (ca. 0.3% of the total Ni), presumably formed at room temperature after the acid etching, not becoming thicker at 300 °C. All catalysts containing Ru (but no CeO$_2$) showed a larger hydrogen consumption (Table 1) due to the presence of additional signals in the low temperature region of their H$_2$-TPR profiles, which can be assigned to the reduction of RuO$_x$ species formed during the oxidative pretreatment [8]. In particular, the main peak broadened and its maximum shifted down to 260–265 °C and it was accompanied by a poorly resolved low temperature shoulder peaking at around 185–200 °C. It is also possible that the presence of Ru favored a larger formation of NiO during the oxidative pretreatment of the foams. Unfortunately, a correct estimation of the corresponding H$_2$ consumption was precluded, because the peaks related to RuO$_x$ partly overlapped with the reduction of NiO, which can be possibly affected (enhanced) by the presence of Ru via a H$_2$-spillover effect that was already reported for similar Ni foams modified with either Rh or Pt [18]. Notably, the reduction of RuO$_x$ started at as low as 85 °C and occurred over a larger temperature range for the Ru/Ni-PED sample compared to its Ru/Ni counterpart prepared by direct impregnation that, on the other hand, required ca. 160 °C to start being reduced: according to XRD and SEM analysis, this effect is possibly due to the amorphous nature of those Ru nanostructures formed during the pulsed electrodeposition.

Figure 4. H_2-TPR plots for Ru/Ni, Ce_x/Ni and Ru/Ce_x/Ni foam catalysts and their bare Ni support following a 1 h oxidative pretreatment in air at 300 °C.
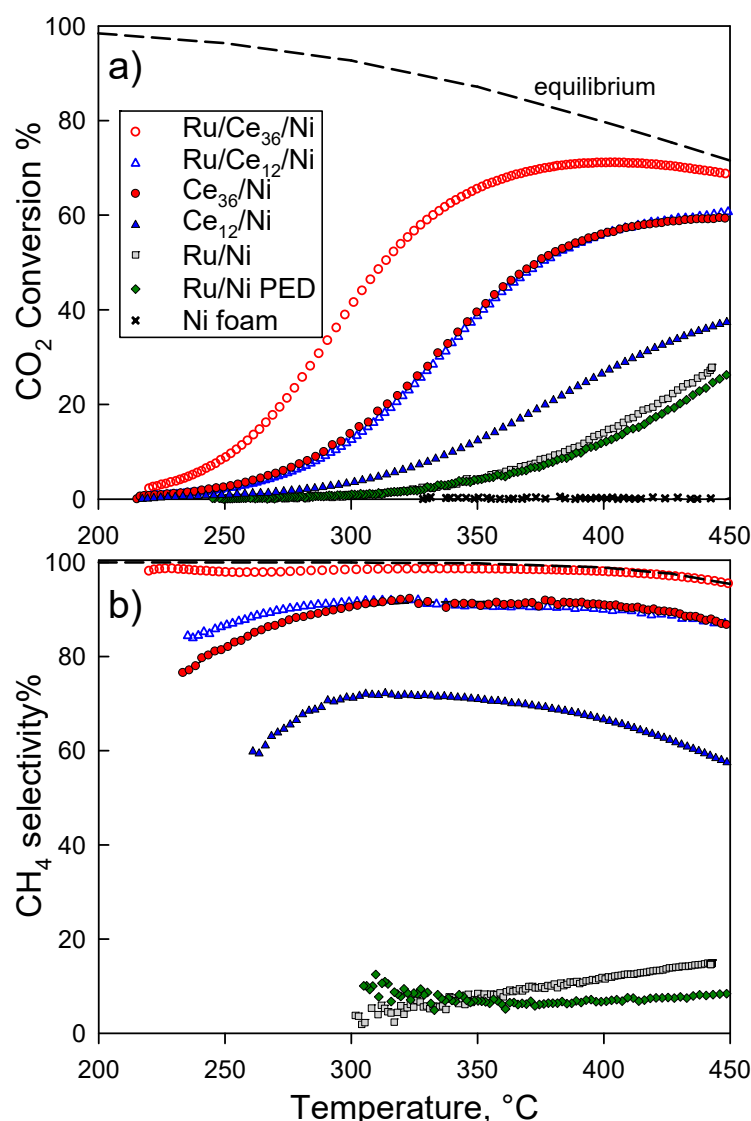
The addition of the CeO_2 layer on the Ni foam increased the total H_2 uptake (per gram of sample, Table 1) and shifted the peak temperature for reduction of superficial NiO down to ca. 270 °C, suggesting a significant interaction between the two layers. While it is generally accepted that surface reduction of CeO_2 to Ce_2O_3 by H_2 occurs in the temperature range between 300 and 600 °C [42,43] it can be argued that the close interaction with the underlying Ni, which is easily accessible to gases, facilitated the reduction process [9], once again via a spill-over effect of H_2 from Ni to CeO_2. Therefore, the reduction of NiO partially overlapped with the reduction of the CeO_2 fraction in close contact with the foam support.

The further addition of Ru on Ce_x/Ni foams significantly enhanced the low temperature reduction peak centered at ca. 190 °C (and starting from ca. 100 °C), which became the main reduction event in the TPR profile for Ru/Ce_{36}/Ni catalyst (Figure 4). On the contrary, the second reduction event was less affected by the presence of Ru and resembled that recorded for Ce_x/Ni systems, though the peak temperature was slightly lower (ca. 250–260 °C). Considering that Ru loading in the two Ru/Ce_x/Ni composite catalysts (as well as in the Ru-Ni sample prepared by impregnation) was nominally identical, it follows that an even stronger interaction existed between Ru and CeO_2 that caused the simultaneous reduction of RuO_x and CeO_2 at low temperature by promoting the extensive formation of oxygen vacancies and/or surface OH groups on CeO_2 [8,42].
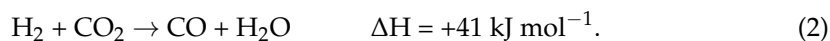
2.2. Catalytic Tests

The CO_2 hydrogenation activity of structured metal foam catalysts was investigated at atmospheric pressure under a steady feed flow of CO_2/H_2/N_2 = 1/4/5 by volume. Figure 5 presents the results in terms of CO_2 conversion and CH_4 selectivity as a function of the reaction temperature (varied in the range 200–450 °C), compared with the corresponding values predicted by thermodynamic equilibrium (at constant T and P).

Bare Ni foams did not show any measurable catalytic activity under the experimental conditions explored in this work, which was in good agreement with previously reported results [23].

Figure 5. CO_2 conversion (**a**) and CH_4 selectivity (**b**) as a function of the reaction temperature during the hydrogenation of CO_2 over foam catalysts. Feed: $CO_2/H_2/N_2 = 1/4/5$. Dashed lines represent thermodynamic equilibrium values (at constant T and P).

Generally, the direct deposition of Ru on the Ni foams promoted the conversion of CO_2 starting from above 300 °C and monotonically increasing up to a maximum of ca. 25% at 450 °C, well below the corresponding thermodynamic equilibrium value. Notably, those foam catalysts prepared by direct impregnation with a Ru nitrosyl nitrate solution gave results quite similar to those of samples prepared by a pulsed electrodeposition method, in spite of their significantly different nominal loadings (see Table 1) and specific surface area of Ru, which, however, remained quite low (below that of the Ni foam). In particular, both types of catalysts displayed a rather low selectivity towards the formation of CH_4, which slightly increased with the reaction temperature but remained below 15% in the whole temperature range. It can be argued that when Ru was in direct contact with the Ni foam, the main product of CO_2 hydrogenation was CO rather than CH_4, indicating the activation of the reverse water gas shift reaction (RWGS, Equation (2)) although the Sabatier reaction (Equation (1)) was thermodynamically favored (as shown by the equilibrium curve in Figure 5b which remains above 99% up to 400 °C).

$$H_2 + CO_2 \rightarrow CO + H_2O \qquad \Delta H = +41 \text{ kJ mol}^{-1}. \tag{2}$$

Unsupported CeO_2 powders were reported to have little activity toward CO_2 hydrogenation and no CH_4 selectivity under similar experimental conditions [43]. However, it is well known that nanometric Ni supported on CeO_2 is an active catalyst for the methanation of CO_2 (and CO) [5,6,43]. Although two types of mechanisms have been suggested for CO_2 methanation on supported metal catalysts [42] (having CO or formates as the main intermediate species), it is generally accepted that H_2 is dissociatively adsorbed on the metal, whereas CO_2 is mainly adsorbed and activated on oxygen vacancies of CeO_2 which are being restored via reduction of the oxide surface in order to close the catalytic cycle [42]. Whatever the intermediate species deriving from the adsorbed CO_2, it has to finally spill over from CeO_2 to Ni (or Ru) to complete the hydrogenation forming CH_4, and therefore the interface between the two phases plays an important role [9]. In order to investigate whether the same reaction mechanism could be active at the interface between a Ni foam and an electrodeposited CeO_2 layer, we tested Ce_{12}/Ni and Ce_{36}/Ni foams and the results are presented in Figure 5. We found that the electrodeposition of a thin porous CeO_2 layer on the struts of the Ni foam was effective to promote the hydrogenation of CO_2. The CO_2 conversion plots over Ce_x/Ni catalysts shifted towards lower temperatures along with the increase in the oxide loading: this suggests either the formation of a larger number of accessible active sites located at the interface between CeO_2 and Ni foam, or a larger availability of adsorption sites on CeO_2 for the activation of CO_2 and formation of intermediate species which can easily migrate towards the (Ni metal) hydrogenation sites. Unfortunately, it was not possible to measure the extent of the Ni-CeO_2 interface by cyclic voltammetry due to the insulating nature of the oxide layer. Finally, we also observed a significant increase in process selectivity to CH_4 that raised from 60% to 70% for Ce_{12}/Ni up to 80–90% for Ce_{36}/Ni.
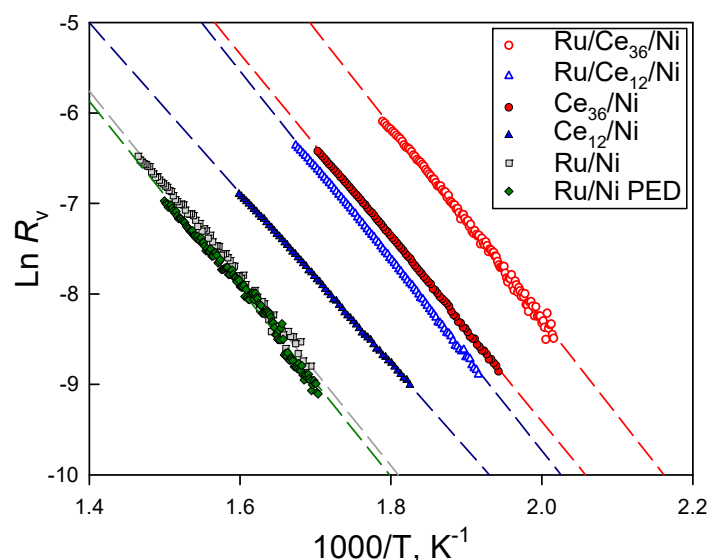
As shown in Figure 5a, the interposition of thin CeO_2 porous layers on the struts of the Ni foam before the deposition of Ru further enhanced the methanation activity of the composite catalysts. The CO_2 conversion level attained over each Ru/Ce_x/Ni foam catalyst at any temperature was higher than over the corresponding Ce_x/Ni samples with the same oxide content and much higher than over Ru/Ni foams with the same Ru loading. Moreover, also in this case, the catalytic activity increased along with the loadings of CeO_2 on the foam catalysts having a fixed content of Ru, following the same trend of reducibility found in TPR experiments. In particular, for the best performing Ru/Ce_{36}/Ni catalyst, CO_2 conversion increased from ca. 2% at 220 °C up to 71% at 400 °C, where it leveled-off before it started to decrease at higher temperatures closely following the trend of its thermodynamic equilibrium value. Figure 5b shows that the Ru/Ce_{36}/Ni catalyst converted CO_2 into methane showing a high selectivity (in the range 98–99%), which closely followed the trend predicted by thermodynamic equilibrium, thus starting to decrease for temperatures above 350 °C due to the formation of increasing amounts of CO via the RWGS reaction (Equation (2)). This agrees well with previous reports on high-performance Ru/CeO_2 catalysts tested under similar conditions [28].

Therefore, it can be concluded that the interposition of CeO_2 showed a marked promoting effect both for the CO_2 methanation activity of Ru sites and for the underlying Ni foam. This is further confirmed considering that the selectivity to CH_4 decreased to the range 87–91% when the ceria loading was reduced to ca. 1/3, at fixed Ru loading (i.e., Ru/Ce_{12}/Ni catalyst), in analogy to the (even larger) drop in selectivity found for Ce_{12}/Ni with respect to Ce_{36}/Ni catalysts. As explained in the Materials and Methods section, we were unable to determine the Ru surface area in Ru/Ce_x/Ni foam catalysts. Thus, we cannot exclude that part of the activity enhancement was due to a geometric factor, besides the Ru–CeO_2 interaction.

The Arrhenius plots (Figure 6) derived from experimental data at low conversion (<10%) show a linear trend for all samples indicating the dominance of a kinetic regime in the specific temperature range selected for each catalyst. Therefore, Table 2 reports values of the apparent activation energy (E_a) calculated from the slopes of Arrhenius plots, the volumetric CO_2 reaction rates measured at 300 °C and the corresponding CH_4 process

selectivity at the same temperature. However, it should be recalled that two reactions, CO_2 methanation and RWGS, run simultaneously under the present conditions. Thus, the estimated values of E_a arise from both reactions, the contribution of which to the activation energy cannot be accurately clarified. Estimates of the intrinsic rates of CO_2 consumption at 300 °C per unit of surface area of foam catalysts as well as per gram of Ru (normalized with respect to the reference Ru/Ni foam) are also presented in the same table.

Figure 6. Arrhenius plots for the specific (volumetric) rate of CO_2 consumption during its hydrogenation over foam catalysts. Feed $CO_2/H_2/N_2 = 1/4/5$ by volume.

Table 2. Apparent activation energy values for the hydrogenation of CO_2 over foam catalysts; process selectivity to CH_4 and CO_2 reaction rates at 300 °C per unit volume and surface area of foam catalysts and per gram of Ru (normalized w.r.t. the value measured over Ru/Ni at the same temperature).

Catalyst	E_a kJ mol^{-1}	CH_4 Selectivity %	CO_2 React. Rate mmol dm^{-3} s^{-1}	CO_2 React. Rate mmol m^{-2} s^{-1}	Normalized CO_2 React. Rate per g of Ru
Ru/Ni	85.1	6.5	0.09	-	1
Ru/Ni PED	85.8	10.1	0.08	-	2.4
Ru/Ce$_{12}$/Ni	87.0	91.6	0.86	2.1	9.2
Ru/Ce$_{36}$/Ni	87.5	98.2	3.80	4.1	42.3
Ce$_{36}$/Ni	84.5	90.6	1.13	0.6	-
Ce$_{12}$/Ni	80.1	71.9	0.26	0.7	-

In particular, the apparent activation energy values for CO_2 consumption measured for the foam catalysts containing Ru were quite similar to each other (86.3 ± 1.1 kJ mol^{-1}), suggesting that all these catalysts obey the same reaction mechanism and have the same rate limiting step [28,44]. In fact, Ce$_x$/Ni catalysts also showed similar values (82.3 ± 3.1 kJ mol^{-1}) of apparent activation energy. This agrees well with previous literature reports on Ru/CeO$_2$ and Ni/CeO$_2$ catalysts suggesting that the activation of CO_2 on oxygen vacancies of CeO$_2$ is the common rate determining step for both type of systems [42].
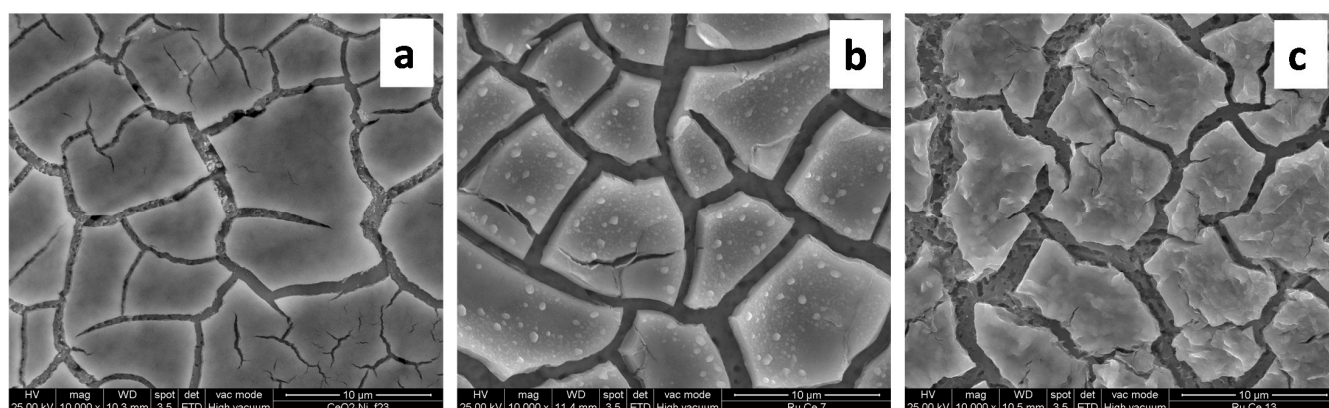
Accordingly, the common value of E_a estimated in this work is very close to what was generally reported for the formation of CO on Ru/Al$_2$O$_3$ (ca. 82 kJ mol^{-1}) that is only slightly higher than the values reported for the production of methane on supported Ru catalysts [45]. However, our data show a high process selectivity towards the production of CO rather than CH_4 when Ru was directly deposited on bare Ni foams and the overall activity is low. On the contrary, the presence of CeO$_2$ strongly promoted the reaction route towards methane, without altering the apparent activation energy. The increase of

selectivity and yield to CH_4 rather than CO along with the increase in the load of CeO_2 at fixed inlet gas flow rate agrees with a reaction mechanism involving CO as reaction intermediate [9], and a CH_4 formation rate which is controlled by the conversion of CO_2 to CO [46,47] under the experimental conditions explored in this study.

After normalization of the reaction rate data for the surface area of Ce_x/Ni and $Ru/Ce_x/Ni$ foams (Table 2) it results that both Ce_x/Ni samples achieve a similar performance, whereas this figure is higher for $Ru/Ce_{12}/Ni$ and $Ru/Ce_{36}/Ni$ by a factor ca. 3 and 6, respectively. It can be argued that relatively high Ce/Ru ratios are required to effectively disperse the noble metal and, in turn, to maximize the number of catalytic active sites at a fixed Ru loading. As a consequence, the CO_2 reaction rate scaled with the oxide loading in the catalyst and increased by a factor as high as 42 when referred to the unit mass of the noble metal (Table 2). It also results that Ru nanostructures formed by the PED method displayed a faster CO_2 consumption rate per gram of metal (by a factor ca. 2.4) with respect to their counterparts obtained by a simple impregnation method, most probably related to the larger exposed specific surface area of the former.

Comparing (volumetric) reaction rate data for Ce_x/Ni and $Ru/Ce_x/Ni$ foams vs. Ni and Ru/Ni foams, it appears clear that the enhanced catalytic activity is caused by the simultaneous development of active sites both at the Ru/CeO_2 and CeO_2/Ni interfaces. Notably, the order of catalytic performance among foam catalysts follow the same trend of reducibility measured by H_2-TPR experiments. This result confirms the key role of a strong interaction between both Ru and Ni with CeO_2 in order to provide a large number of easily regenerable oxygen vacancies on the surface of the oxide where CO_2 is activated [1,9,44].

Ce_x/Ni and $Ru/Ce_x/Ni$ catalysts were inspected again with SEM after the catalytic tests. Figure 7a shows the formation of many cracks in Ce_{12}/Ni, but an essentially unaltered well-adhered ceria layer on most of the Ni surface. As for $Ru/Ce_{12}/Ni$, in addition to enhanced cracking, Figure 7b shows the formation of Ru enriched nuclei of various characteristic sizes up to ca. 1 μm wide not detectable for the as-prepared catalyst (Figure 2c). This suggest the occurrence of metal sintering during operation at temperature up to 450 °C that is most probably due to the relatively low Ce/Ru ratio in those catalysts. Indeed, the behavior of Ce_{36}/Ni and $Ru/Ce_{36}/Ni$ (Figure 7c) was similar, but the formation of Ru nuclei was not observed, because in the as-prepared sample Ru was more effectively dispersed in the pores of the thicker CeO_2 layer and thus metal sintering was prevented. Nevertheless, the partial detachment of the oxide layer at higher loadings obviously reduced the contact area between Ni and CeO_2.

Figure 7. SEM images of Ce_{12}/Ni (**a**), $Ru/Ce_{12}/Ni$ (**b**), and $Ru/Ce_{36}/Ni$ (**c**) recorded after methanation tests.

Given the limited adhesion of thick CeO_2 overlayers on the struts of the Ni foam precluding high oxide loadings on the catalysts, and considering the evident benefit in terms of intrinsic methanation activity and selectivity deriving from a relatively high dispersion of Ru in the pores of CeO_2 as well as from the maximization of the interface

between CeO_2 and Ni foam, it follows that room is left for the optimization of the catalyst formulation, which, however, is beyond the scope of the present work.

3. Materials and Methods

3.1. Catalysts Preparation

The Ni foams (75 ppi) were purchased from INCOFOAM ^{TM}. Their specific surface area was determined by cyclic voltammetry carried out in 1.0 M KOH through the measurement of the charge associated with the Ni(II)/Ni(III) system, as described in [41]. The deposition of CeO_2 was carried out in single-compartment cells from 0.100 M $Ce(NO_3)_3$ solutions. Counter electrode was a Pt wire and a Saturated Calomel Electrode (SCE) was the reference. Electrolyses were performed at -1.2 V (SCE) constant potential. Two different deposition charges were used (12 C cm^{-3} and 36 C cm^{-3}) and the actual loading of CeO_2 was estimated by the weight increase of the samples. All electrochemical experiments were performed with an Autolab PGSTAT 302 N (Autolab, Utrecht, Netherlands). Ru was deposited by dropwise addition of 0.25 mL of a Ru(III) nitrosyl nitrate water solution (1.4% wt. of Ru, Aldrich) leading to a nominal noble metal loading of 7.3 mg$_{Ru}$ cm^{-3}. Impregnated foams were dried at 120 °C for 12 h in air and finally reduced at 450 °C for 1 h under a flow of 20% vol. H_2/N_2. Ru/Ni catalysts were prepared with a similar procedure by the dropwise addition of the Ru(III) nitrosyl nitrate solution to bare Ni foam samples. In this case, the noble metal load was confirmed to be within $\pm 10\%$ of its nominal value by the weight increase of the samples. Other CeO_2-free catalysts, henceforth called Ru/Ni-PED, were prepared by submitting Ni foams to pulsed electrodeposition of Ru. Foam samples were immersed in 0.002 M $RuCl_3$ + 1 M NaCl solutions, at pH 2.0, 25 °C, and their potential was pulsed between $E_1 = -0.8$ V (SCE) and $E_2 = 0.0$ V (SCE) during $t_1 = 0.1$ s and $t_2 = 0.3$ s for 1000 cycles. Unlike Ru/Ni, Ru/Ni-PED catalysts underwent no thermal treatment. For both samples, the surface area of Ru was evaluated the by recording cyclic voltammograms in 1.0 M KOH, measuring the charge associated to H desorption and comparing it with the corresponding charge measured on a quasi-ideally flat Ru electrode [48]. This method requires that the Ru deposits be in electrical contact with the Ni foam. For this reason, it could not be applied to Ru/Ce$_x$/Ni samples where the Ru nano-particles were dispersed in the electrically insulating CeO_2 layers.

3.2. Catalysts Characterization

Scanning electron microscopy (SEM) images were obtained with a FEI-Quanta 200 FEM ESEM instrument (Thermo Fisher Scientific, Waltham, MA, USA) and a Zeiss-SIGMA instrument (ZEISS, Oberkochen, Germany), both equipped with a field emission gun, operating at an accelerating voltage variable between 10 and 30 kV under high vacuum conditions. Energy Dispersive Spectroscopy analyses (EDS), used to confirm the presence of specific elements (Ru and Ce) in the deposits formed on the Ni foams, were performed with an EDAX Genesis System (Ametek Materials Analysis Division) in the case of FEI-Quanta instrument and with and Oxford X-MAX apparatus (Oxford Instruments, Oxford, UK) in the case of Zeiss-SIGMA instrument.

X-ray diffraction (XRD) patterns were collected by using a Philips X-PERT PW3710 diffractometer (Philips, Amsterdam, the Netherlands) with a Bragg–Brentano geometry, employing a CuKa source (40 kV, 30 mA). Ahead of the XRD analyses, the foams were compressed to obtain flat, ca. 0.5 mm thick samples.

The textural properties of Ce$_x$/Ni and Ru/Ce$_x$/Ni catalysts were determined by N_2 adsorption at -196 °C using a Quantachrome Autosorb 1-C instrument analyzer (Quantachrome Instruments, Boynton Beach, FL, USA). Foam samples were degassed under high vacuum at 150 °C for 3 h ahead of analyses. The BET method (P/P_0 range from 0.08 to 0.2) was adopted for the calculation of the specific surface area (S.S.A.); the pore size distribution (PSD) was evaluated via the NL-DFT (cylindrical pore) model applied to the desorption branch of the isotherm.

H_2 temperature programmed reduction (TPR) experiments were performed with a Micromeritics AutoChem 2020 (Micromeritics, Norcross, GA, USA) equipped with a TC detector. Samples of foam catalysts (70–100 mg) were pre-oxidized in-situ under an air flow at 300 °C for 1 h, then cooled to room temperature and finally reduced under a 5%H_2/Ar flow (50 cm^3 min^{-1}) ramping the temperature up to 600 °C at 10 °C min^{-1}.

3.3. Catalytic Testing

The catalytic hydrogenation of CO_2 was investigated in a fixed-bed quartz tubular reactor (d_{in} = 20 mm) operated under atmospheric pressure and externally heated by an electric oven [13]: 5/6 metal foam disks were stacked together and wrapped with a ceramic tape to prevent the by-pass of gas along the inner walls of the reactor. Two K-type thermocouples were used to measure the reaction temperature of the front and back catalytic foams of the stack. The catalysts were pre-reduced in-situ under a flow of 20% vol. H_2/N_2 at 450 °C before testing. The feed composition was adjusted to CO_2/H_2/N_2 = 1/4/5 (by vol.) by premixing calibrated fluxes of high-purity gases (CO_2, H_2, N_2) using three independent mass flow controllers (mod. 5850 Brooks Instrument, Veenendaal, the Netherlands): the total inlet flow rate set at 20 SL h^{-1}, corresponding to a Gas Hourly Space Velocity (GHSV) = 6600–7870 h^{-1} based on the volume of the foams. Reaction tests were run in the temperature programmed mode by ramping the temperature up to 450 °C at 3 °C min^{-1}. The concentrations of CO, CO_2, CH_4, and H_2 were measured in real-time using a gas analyzer with cross-sensitivity corrections (Optima Advance, ABB, Zurich, Switzerland) after removing water through a chiller and a $CaCl_2$ trap [49].

The conversion of CO_2 and the corresponding process selectivity to CH_4 were calculated according to following definitions based on measured dry molar fractions of CO_2, CH_4, and CO in the products, considering the eventual formation of traces of higher hydrocarbons negligible [46]:

$$x_{CO2} = 100\left(1 - \frac{CO_2^{out}}{CO_2^{out} + CH_4^{out} + CO^{out}}\right), \tag{3}$$

$$s_{CH4} = 100\left(\frac{CH_4^{out}}{CH_4^{out} + CO^{out}}\right). \tag{4}$$

The Gaseq software was employed to evaluate equilibrium conversion and selectivity values at constant temperature and pressure.

The CO_2 consumption rate per unit volume of catalytic foams (R_vCO_2) was estimated under the assumption of an isothermal plug flow reactor working under differential conditions and constant molar flow rate: low conversion data (<10%, ΔT_{out-in} < 5 °C) far from equilibrium were used for the calculations. Arrhenius plots for R_vCO_2 were used to estimate the apparent activation energy of the catalytic hydrogenation of CO_2 [49].

4. Conclusions

Novel structured catalysts were prepared starting from a commercial 3D open cell Ni foam with high pore density (75 ppi) onto which a CeO_2 layer was deposited via electroprecipitation, and, eventually, Ru was added by impregnation.

The mesoporous CeO_2 layer, whose thickness was controlled by deposition charge, had specific surface area in the range 45–70 m^2 g^{-1} and covered homogeneously the struts of the Ni foam. The morphology and adherence of the CeO_2 layer were preserved under reaction conditions up to 450 °C if the thickness was low (0.3–1 µm), whereas thicker layers (1.5–3.5 µm) cracked and partially detached from the struts.

Discontinuous layers of amorphous Ru formed in Ru/Ni catalysts prepared by direct impregnation, probably via a Ru-Ni galvanic displacement reaction. More continuous Ru layers were produced by pulsed electrodeposition. In both cases, the surface area of Ru remained below that of Ni, since Ru did not form well-dispersed, large-area nanometric deposits. At variance, Ru was well dispersed in the pores of the CeO_2 layer.

The close interaction of the CeO_2 layer with the underlying Ni foam and the Ru facilitated the reduction process of the oxide via a spill-over effect of H_2 from Ni and Ru to CeO_2, and promoted the extensive formation of oxygen vacancies and/or surface OH groups on CeO_2, which were active sites for the adsorption and activation of CO_2.

The direct deposition of Ru on the Ni foams promoted the conversion of CO_2 to form mostly CO via the reverse water gas shift reaction. The electrodeposition of the CeO_2 layer on the Ni foam effectively promoted the hydrogenation of CO_2, with the process selectivity to methane increasing along with the CeO_2 loading. The deposition of Ru further enhanced the methanation activity following the same order of reducibility found in H_2-TPR experiments.

The presence of CeO_2 strongly enhanced the yield and selectivity to methane, without altering the apparent activation energy: this suggests that the activation of CO_2 on oxygen vacancies is the rate determining step and CH_4 formation proceeds via a CO intermediate route.

Considering their outstanding mass- and heat-transfer features, $Ru/Ce_x/Ni$ foam catalysts appear to be particularly suited for the intensification of highly exothermic catalytic processes operating under external mass transfer limitations, i.e., when the drawback of a limited volumetric loading of the catalytic active phase does not represent a critical issue.

Supplementary Materials: The following are available online at https://www.mdpi.com/2073-4344/11/1/13/s1, Figure S1: SEM images of Ce_{36}/Ni and $Ru/Ce_{36}/Ni$; Figure S2: SEM images of as-prepared Ru/Ni and Ru/Ni-PED; Figure S3: Cyclic voltammograms recorded with Ru/Ni and Ru/Ni PED catalysts; Figure S4: XRD spectra of Ce_{32}/Ni, $Ru/Ce_{32}/Ni$, Ru/Ni, Ru/Ni PED, and bare Ni foam.

Author Contributions: Conceptualization: S.C. and L.V.-G.; data curation: S.C., E.M.C., S.F., and L.V.-G.; formal analysis: S.C., L.L., and L.V.-G.; funding acquisition: S.C.; investigation: S.C., E.M.C., and L.V.-G.; project coordination: S.C.; supervision: S.C. and M.M.; writing—original draft: S.C., L.V.-G., and M.M.; writing—review & editing, L.L., M.M., and L.V.-G. All authors have read and agreed to the published version of the manuscript.

Data Availability Statement: The data presented in this study are available on request from the corresponding author.

Conflicts of Interest: The authors declare no conflict of interest.

References

1. Ghaib, K.; Ben-Fares, F.Z. Power-to-Methane: A state-of-the-art review. *Renew. Sustain. Energy Rev.* **2018**, *81*, 433–446. [CrossRef]
2. Vogt, C.; Monai, M.; Kramer, G.J.; Weckhuysen, B.M. The renaissance of the Sabatier reaction and its applications on Earth and in space. *Nat. Catal.* **2019**, *2*, 188–197. [CrossRef]
3. Artz, J.; Müller, T.E.; Thenert, K.; Kleinekorte, J.; Meys, R.; Sternberg, A.; Bardow, A.; Leitner, W. Sustainable Conversion of Carbon Dioxide: An Integrated Review of Catalysis and Life Cycle Assessment. *Chem. Rev.* **2018**, *118*, 434–504. [CrossRef] [PubMed]
4. Nguyen, T.T.M.; Wissing, L.; Skjøth-Rasmussen, M.S. High temperature methanation: Catalyst considerations. *Catal. Today* **2013**, *215*, 233–238. [CrossRef]
5. Ricca, A.; Truda, L.; Palma, V. Study of the role of chemical support and structured carrier on the CO_2 methanation reaction. *Chem. Eng. J.* **2018**, *377*, 120461. [CrossRef]
6. Fukuhara, C.; Hayakawa, K.; Suzuki, Y.; Kawasaki, W.; Watanabe, R. A novel nickel-based structured catalyst for CO_2 methanation: A honeycomb-type Ni/CeO_2 catalyst to transform greenhouse gas into useful resources. *Appl. Catal. A Gen.* **2017**, *532*, 12–18. [CrossRef]
7. Li, Y.; Zhang, Q.; Chai, R.; Zhao, G.; Liu, Y.; Lu, Y. Structured $Ni-CeO_2-Al_2O_3$/Ni-Foam Catalyst with Enhanced Heat Transfer for Substitute Natural Gas Production by Syngas Methanation. *ChemCatChem* **2015**, *7*, 1427–1431. [CrossRef]
8. Nguyen, H.T.T.; Kumabe, Y.; Ueda, S.; Kan, K.; Ohtani, M.; Kobiro, K. Highly durable Ru catalysts supported on CeO_2 nanocomposites for CO_2 methanation. *Appl. Catal. A Gen.* **2019**, *577*, 35–43. [CrossRef]
9. Lee, S.M.; Lee, Y.H.; Moon, D.H.; Ahn, J.Y.; Nguyen, D.D.; Chang, S.W.; Kim, S.S. Reaction Mechanism and Catalytic Impact of Ni/CeO_{2-x} Catalyst for Low-Temperature CO_2 Methanation. *Ind. Eng. Chem. Res.* **2019**, *58*, 8656–8662. [CrossRef]

10. Giani, L.; Groppi, G.; Tronconi, E. Mass-Transfer Characterization of Metallic Foams as Supports for Structured Catalysts. *Ind. Eng. Chem. Res.* **2005**, *44*, 4993–5002. [CrossRef]

11. Lucci, F.; Della Torre, A.; Montenegro, G.; Dimopoulos Eggenschwiler, P. On the catalytic performance of open cell structures versus honeycombs. *Chem. Eng. J.* **2015**, *264*, 514–521. [CrossRef]

12. Cimino, S.; Gambirasi, A.; Lisi, L.; Mancino, G.; Musiani, M.; Vázquez-Gómez, L.; Verlato, E. Catalytic combustion of methanol on Pt-Fecralloy foams prepared by electrodeposition. *Chem. Eng. J.* **2015**, *285*, 276–285. [CrossRef]

13. Verlato, E.; Barison, S.; Cimino, S.; Lisi, L.; Mancino, G.; Musiani, M.; Paolucci, F. Electrochemical preparation of nanostructured CeO_2-Pt catalysts on Fe-Cr-Al alloy foams for the low-temperature combustion of methanol. *Chem. Eng. J.* **2017**, *317*, 551–560. [CrossRef]

14. Ho, P.H.; Ambrosetti, M.; Groppi, G.; Tronconi, E.; Jaroszewicz, J.; Ospitali, F.; Rodriguez-Castellon, E.; Fornasari, G.; Vaccari, A.; Benito, P. One-step electrodeposition of Pd-CeO_2 on high pore density foams for environmental catalytic processes. *Catal. Sci. Technol.* **2018**, *8*, 4678–4689. [CrossRef]

15. Zhang, Z.; Ding, J.; Chai, R.; Zhao, G.; Liu, Y.; Lu, Y. Oxidative dehydrogenation of ethane to ethylene: A promising CeO_2-ZrO_2-modified NiO-Al_2O_3/Ni-foam catalyst. *Appl. Catal. A Gen.* **2018**, *550*, 151–159. [CrossRef]

16. Benito, P.; Nuyts, G.; Monti, M.; De Nolf, W.; Fornasari, G.; Janssens, K.; Scavetta, E.; Vaccari, A. Stable Rh particles in hydrotalcite-derived catalysts coated on FeCrAlloy foams by electrosynthesis. *Appl. Catal. B Environ.* **2015**, *179*, 321–332. [CrossRef]

17. Ho, P.H.; De Nolf, W.; Ospitali, F.; Beton, D.; Torkuhl, L.; Fornasari, G.; Vaccari, A.; Benito, P. Insights into coated NiCrAl open-cell foams for the catalytic partial oxidation of CH_4. *React. Chem. Eng.* **2019**, *4*, 1768–1778. [CrossRef]

18. Cimino, S.; Lisi, L.; Mancino, G.; Musiani, M.; Vázquez-Gómez, L.; Verlato, E. Catalytic partial oxidation of CH_4–H_2 mixtures over Ni foams modified with Rh and Pt. *Int. J. Hydrogen Energy* **2012**, *37*, 17040–17051. [CrossRef]

19. Coleman, L.J.I.; Croiset, E.; Epling, W.; Fowler, M.; Hudgins, R.R. Evaluation of Foam Nickel for the Catalytic Partial Oxidation of Methane. *Catal. Lett.* **2008**, *128*, 144–153. [CrossRef]

20. Verlato, E.; Barison, S.; Cimino, S.; Dergal, F.; Lisi, L.; Mancino, G.; Musiani, M.; Vázquez-Gómez, L. Catalytic partial oxidation of methane over nanosized Rh supported on Fecralloy foams. *Int. J. Hydrogen Energy* **2014**, *39*, 11473–11485. [CrossRef]

21. Frey, M.; Bengaouer, A.; Geffraye, G.; Edouard, D.; Roger, A.C. Aluminum Open Cell Foams as Efficient Supports for Carbon Dioxide Methanation Catalysts: Pilot-Scale Reaction Results. *Energy Technol.* **2017**, *5*, 2078–2085. [CrossRef]

22. Huynh, H.L.; Yu, Z. CO_2 Methanation on Hydrotalcite-Derived Catalysts and Structured Reactors: A Review. *Energy Technol.* **2020**, *8*, 1901475. [CrossRef]

23. Li, Y.; Zhang, Q.; Chai, R.; Zhao, G.; Liu, Y.; Lu, Y.; Cao, F. Ni-Al_2O_3/Ni-foam catalyst with enhanced heat transfer for hydrogenation of CO_2 to methane. *AIChE J.* **2015**, *61*, 4323–4331. [CrossRef]

24. Li, Y.; Zhang, Q.; Chai, R.; Zhao, G.; Cao, F.; Liu, Y.; Lu, Y. Metal-foam-structured Ni-Al_2O_3 catalysts: Wet chemical etching preparation and syngas methanation performance. *Appl. Catal. A Gen.* **2016**, *510*, 216–226. [CrossRef]

25. Montebelli, A.; Visconti, C.G.; Groppi, G.; Tronconi, E.; Kohler, S.; Venvik, H.J.; Myrstad, R. Washcoating and chemical testing of a commercial Cu/ZnO/Al_2O_3 catalyst for the methanol synthesis over copper open-cell foams. *Appl. Catal. A Gen.* **2014**, *481*, 96–103. [CrossRef]

26. Polanski, J.; Lach, D.; Kapkowski, M.; Bartczak, P.; Siudyga, T.; Smolinski, A. Ru and Ni—Privileged Metal Combination for Environmental Nanocatalysis. *Catalysts* **2020**, *10*, 992. [CrossRef]

27. Le, T.A.; Kim, M.S.; Lee, S.H.; Kim, T.W.; Park, E.D. CO and CO2 methanation over supported Ni catalysts. *Catal. Today* **2017**, *293–294*, 89–96. [CrossRef]

28. Tada, S.; Shimizu, T.; Kameyama, H.; Haneda, T.; Kikuchi, R. Ni/CeO2 catalysts with high CO_2 methanation activity and high CH_4 selectivity at low temperatures. *Int. J. Hydrogen Energy* **2012**, *37*, 5527–5531. [CrossRef]

29. Zhou, Y.; Switzer, J.A. Growth of cerium(IV) oxide films by the electrochemical generation of base method. *J. Alloys Compd.* **1996**, *237*, 1–5. [CrossRef]

30. Aldykiewicz, A.J., Jr.; Davenport, A.J.; Isaacs, H.S. Studies of the formation of cerium-rich protective films using X-Ray absorption near-edge spectroscopy and rotating disk electrode methods. *J. Electrochem. Soc.* **1996**, *143*, 147–154. [CrossRef]

31. Li, F.-B.; Newman, R.C.; Thompson, G.E. In situ atomic force microscopy studies of electrodeposition mechanism of cerium oxide films: Nucleation and growth out of a gel mass precursor. *Electrochim. Acta* **1997**, *42*, 2455–2464. [CrossRef]

32. Fernandes, V.; Klein, J.J.; Schreiner, W.H.; Mattoso, N.; Mosca, D.H. Electrodeposition of nanocrystalline CeO_2 on Si(001). *J. Electrochem. Soc.* **2009**, *156*, E199–E204. [CrossRef]

33. Faisal, F.; Toghan, A.; Khalakhan, I.; Vorokhta, M.; Matolin, V.; Libuda, J. Characterization of thin CeO2 films electrochemically deposited on HOPG. *Appl. Surf. Sci.* **2015**, *350*, 142–148. [CrossRef]

34. Verlato, E.; Barison, S.; Einaga, Y.; Fasolin, S.; Musiani, M.; Nasi, L.; Natsui, K.; Paolucci, F.; Valenti, G. CO_2 reduction to formic acid at low overpotential on BDD electrodes modified with nanostructured CeO_2. *J. Mater. Chem. A* **2019**, *7*, 17896–17905. [CrossRef]

35. Creus, J.; Brezault, F.; Rebere, C.; Gadouleau, M. Synthesis and characterisation of thin cerium oxide coatings elaborated by cathodic electrolytic deposition on steel substrate. *Surf. Coat. Technol.* **2006**, *200*, 4636–4645. [CrossRef]

36. Hamlaoui, Y.; Pedraza, F.; Tifouti, L. Investigation of electrodeposited cerium oxide based films on carbon steel and of the induced formation of carbonated green rusts. *Corros. Sci.* **2008**, *50*, 2182–2188. [CrossRef]

37. Hamlaoui, Y.; Pedraza, F.; Remazeilles, C.; Cohendoz, S.; Rébéré, C.; Tifouti, L.; Creus, J. Cathodic electrodeposition of cerium-based oxides on carbon steel from concentrated cerium nitrate solutions Part I. Electrochemical and analytical characterization. *Mater. Chem. Phys.* **2009**, *113*, 650–657. [CrossRef]

38. Hamlaoui, Y.; Tifouti, L.; Remazeilles, C.; Pedraza, F. Cathodic electrodeposition of cerium based oxides on carbon steel from concentrated cerium nitrate. Part II: Influence of electrodeposition parameters and of the addition of PEG. *Mater. Chem. Phys.* **2010**, *120*, 172–180. [CrossRef]

39. Bouchaud, B.; Balmain, J.; Bonnet, G.; Pedraza, F. Optimizing structural and compositional properties of electrodeposited ceria coatings for enhanced oxidation resistance of a nickel-based superalloy. *Appl. Surf. Sci.* **2013**, *268*, 218–224. [CrossRef]

40. Bouchaud, B.; Balmain, J.; Bonnet, G.; Pedraza, F. Correlations between electrochemical mechanisms and growth of ceria based coatings onto nickel substrates. *Electrochim. Acta* **2013**, *88*, 798–806. [CrossRef]

41. Verlato, E.; Cattarin, S.; Comisso, N.; Gambirasi, A.; Musiani, M.; Vázquez-Gómez, L. Preparation of Pd-Modified Ni Foam Electrodes and Their Use as Anodes for the Oxidation of Alcohols in Basic Media. *Electrocatalysis* **2012**, *3*, 48–58. [CrossRef]

42. Sakpal, T.; Lefferts, L. Structure-dependent activity of CeO_2 supported Ru catalysts for CO_2 methanation. *J. Catal.* **2018**, *367*, 171–180. [CrossRef]

43. Atzori, L.; Cutrufello, M.G.; Meloni, D.; Cannas, C.; Gazzoli, D.; Monaci, R.; Sini, M.F.; Rombi, E. Highly active NiO-CeO_2 catalysts for synthetic natural gas production by CO_2 methanation. *Catal. Today* **2018**, *299*, 183–192. [CrossRef]

44. Wang, F.; Li, C.; Zhang, X.; Wei, M.; Evans, D.G.; Duan, X. Catalytic behavior of supported Ru nanoparticles on the {100}, {110}, and {111} facet of CeO_2. *J. Catal.* **2015**, *329*, 177–186. [CrossRef]

45. Kwak, J.H.; Kovarik, L.; Szanyi, J. CO_2 Reduction on Supported Ru/Al_2O_3 Catalysts: Cluster Size Dependence of Product Selectivity. *ACS Catal.* **2013**, *3*, 2449–2455. [CrossRef]

46. Falbo, L.; Martinelli, M.; Visconti, C.G.; Lietti, L.; Bassano, C.; Deiana, P. Kinetics of CO2 methanation on a Ru-based catalyst at process conditions relevant for Power-to-Gas applications. *Appl. Catal. B Environ.* **2018**, *225*, 354–363. [CrossRef]

47. Janke, C.; Duyar, M.S.; Hoskins, M.; Farrauto, R. Catalytic and adsorption studies for the hydrogenation of CO_2 to methane. *Appl. Catal. B Environ.* **2014**, *152–153*, 184–191. [CrossRef]

48. Woods, R. Chemisorption at electrodes: Hydrogen and oxygen on noble metals and their alloys. In *Electroanalytical Chemistry*; Bard, A.J., Ed.; Marcel Dekker: New York, NY, USA, 1976; Volume 9, p. 1.

49. Cimino, S.; Boccia, F.; Lisi, L. Effect of alkali promoters (Li, Na, K) on the performance of Ru/Al_2O_3 catalysts for CO_2 capture and hydrogenation to methane. *J. CO_2 Util.* **2020**, *37*, 195–203. [CrossRef]